SUPPORTING INFORMATION

Charge Transfer Phase Transition with Reversed Thermal Hysteresis Loop in the Mixed-Valence $Fe_9[W(CN)_8]_6 \cdot x$MeOH Cluster

Szymon Chorazy,[a] Robert Podgajny,*[a] Wojciech Nogaś,[a] Wojciech Nitek,[a] Marcin Kozieł,[a] Michał Rams,[b] Ewa Juszyńska-Gałązka,[c] Jan Żukrowski,[d] Czesław Kapusta,[d] Koji Nakabayashi,[e] Takashi Fujimoto,[e] Shin-ichi Ohkoshi[e] and Barbara Sieklucka[a]

[a]*Faculty of Chemistry, Jagiellonian University, Ingardena 3, 30-060 Kraków, Poland. Tel.: (4812) 6632051. E-mail: podgajny@chemia.uj.edu.pl.*
[b]*M. Smoluchowski Institute of Physics, Jagiellonian University, Reymonta 4, 30-059 Kraków, Poland.*
[c]*H. Niewodniczański Institute of Nuclear Physics PAN, Radzikowskiego 152, 31-342 Kraków, Poland.*
[d]*AGH University of Science and Technology, Faculty of Physics and Applied Computer Science, Mickiewicza 30, 30-059 Kraków, Poland.*
[e]*Department of Chemistry, School of Science, The University of Tokyo, 7-3-1 Hongo, Bunkyo-ku, 113-0033 Tokyo, Japan.*

1. Experimental details.

1a. Materials

$Na_3[W^V(CN)_8]\cdot 4H_2O$ was synthesized according to the published procedure.[S1] $Fe^{II}Cl_2\cdot 4H_2O$ and methanol (MeOH) were purchased from commercial sources (Sigma Aldrich, Idalia), and used without purification.

1b. Synthesis and preliminary characterization of 1

The freshly prepared methanolic solution (6 mL) of $FeCl_2\cdot 4H_2O$ (60 mg, 0.3 mmol) was quickly mixed with methanolic solution (3 mL) of $Na_3[W(CN)_8]\cdot 4H_2O$ (107 mg, 0.2 mmol) in a test-tube. The whole mixture was vigorously shaken for several seconds, closed with parafilm, and left for crystallization. The dark green precipitate appeared immediately, and the solution became green. After several days, the tube contained a transparent dark green solution, a precipitate on its bottom, and dark green block crystals of **1** on its walls. It was checked that the same product is obtained under oxygen-free conditions using Schlenk line. The crystals were identified as $\{Fe_9[W(CN)_8]_6(MeOH)_{24}\}\cdot x$MeOH by X-ray monocrystalline diffraction. While washed with MeOH and exposed to the air, they exchange relatively quickly MeOH molecules to H_2O molecules to reach a stable composition $\{Fe_9[W(CN)_8]_6\}\cdot 30H_2O$. The basic characteristics for air-stable phase: *(a)* IR (KBr, cm^{-1}). CN^- stretching vibrations: 2120vs,br, suggesting a domination of $[W^{IV}(CN)_8]^{4-}$ due to the reduction of $[W^V(CN)_8]^{3-}$. MeOH skeletal vibration in 1050-1000 cm^{-1} range disappear, while H_2O vibrations in 1650-1600 cm^{-1} range appear; *(b)* X-ray microanalysis: measured Fe:W molar ratio = 3.08:1.92, which indicates the real ratio Fe:W = 3:2; *(c)* CHN elemental analysis. Anal. Calcd. for $Fe_9W_6C_{48}H_{60}N_{48}O_{30}$: C, 16.98%; H, 1.78%; N, 19.80%. Found: C, 16.95%; H, 1.80%; N, 19.82%.

1c. Crystal structure determination

Single crystal diffraction data of $\mathbf{1}^{HT}$ and $\mathbf{1}^{LT}$ were collected on a Nonius-Bruker KappaCCD four circle diffractometer with graphite monochromated Mo Kα radiation and Oxford CryoJet system for measurements at low temperature. The crystal of $\mathbf{1}^{HT}$ was placed in capillary in atmosphere of solvent, to prevent the loss of the solvent molecules. For the case of $\mathbf{1}^{LT}$, the crystal was coated by apiezonN.oil, and cooled slowly to the indicated temperature. Positions of non-hydrogen atoms were determined using SIR-97.[S2] Non-hydrogen atoms of cluster cores were refined anisotropically using weighted full-matrix least-squares on F^2. Non-hydrogen atoms of solvent molecules were refined isotropically to ensure the convergence of the refinement process. Distances C-O in some methanol molecules were restrained to ensure proper geometry. Restraints on thermal ellipsoids of

atoms of some significantly disordered methanol molecules were also used. All hydrogen atoms joined to carbon atoms were positioned with an idealized geometry and refined using a riding model. The position of hydrogen atoms of some solvent methanol molecules and hydroxyl groups of all methanol molecules were completely unreachable. Refinement and further calculations were carried out using SHELXL-97.[S3] Graphics were created by MERCURY 2.3.[S4]

1d. Physical techniques

To prevent the decomposition of the investigated material, the most of physical measurements were performed on the crystals placed in the mother liquid (**1@MeOH**), or dispersed in apiezonN.oil (**1@ap**). Powder X-ray diffraction patterns of **1@MeOH** sealed in glass capillary (0.5 mm) were collected on a PANalytical X'Pert PRO MPD diffractometer with Debye-Scherrer geometry using CuKα radiation (λ = 1.54187 Å; 2θ range: 3-85° for RT). Non-ambient measurements were performed using the same device with Oxford Cryostream add-on in two modes: cooling (280 K → 150 K) and heating (150 K → 293 K) with proper temperature stabilization time for each measurement (2θ range: 4 – 40°). Cell parameters for RT and 150K were refined using Jana2006 Software[S5] using as starting parameters single crystal data (cell parameters and space group but not cell contents). DSC signals of **1@ap** in the 150 – 300 K range were measured on a Mettler Toledo DSC 822^{e} calorimeter. Magnetic measurements were performed using a Quantum Design SQUID magnetometer. The magnetic data were collected for **1@MeOH**, and were corrected for the diamagnetic contributions using Pascal constants.[S6] ^{57}Fe Moessbauer spectra for **1@ap** were measured on homemade experimental set (AGH University of Science and Technology, Faculty of Physics and Applied Computer Science). CHN elemental analysis for a dried sample of **1** was performed on a EuroEA EuroVector elemental analyser. Molar ratio of *d* metal centers in a dried sample of **1** was determined using Hitachi S-4700 SEM microscope equipped with EDS NORAN Vantage microanalysis system. Room temperature infrared spectra for a dried sample of **1** were measured in KBr pellets on Bruker EQUINOX 55 spectrometer. Variable temperature infrared spectra of **1@ap** were recorded using an EXCALIBUR FTS-3000 spectrometer. During the experiments, the spectrometer was purged with dry nitrogen. The measurements were carried out during cooling and heating with 2-3 K interval. The samples were sandwiched between two KRS-5 window disks. The UV-Vis diffuse reflectance spectra were measured by a Shimadzu UV-3100 spectrometer for **1@ap**. The temperature during the optical spectrum measurements was controlled with the rate of 2 K/min by an Oxford Instruments Microstate-He. After reaching the each temperature, it kept for 5 min to be stabilized before the measurement.

Table S1 Crystal data and structure refinement for **1**^{HT} and **1**^{LT}

compound		**1**^{HT}	**1**^{LT}
method		single-crystal XRD	single-crystal XRD
formula		$Fe_9W_6C_{84.5}H_{145.5}N_{48}O_{36.5}$	$Fe_9W_6C_{90}H_{168}N_{48}O_{42}$
formula weight [g·mol^{-1}]		4024.01	4200.24
T [K]		293(2)	140(2)
λ [Å]		0.71073 (Mo Kα)	0.71073 (Mo Kα)
crystal system		monoclinic	monoclinic
space group		C 2/c	C 2/c
unit cell	***a*** [Å]	28.8360(5)	28.3840(4)
	b [Å]	19.5840(5)	19.0770(3)
	c [Å]	32.8010(5)	32.3450(5)
	β [deg]	113.6570(11)	113.6570(10)
V [Å^3]		16967.0(6)	16022.0(4)
Z		4	4
calculated density [g·cm^{-3}]		1.553	1.718
absorption coefficient [cm^{-1}]		4.860	5.153
F(000)		7612	8004
crystal size [mm × mm × mm]		0.30 × 0.20 × 0.18	0.30 × 0.22 × 0.18
Θ range [deg]		2.08 – 30.04	1.32 – 27.50
limiting indices		-40 < h < 40 -27 < k < 27 -46 < l < 46	-21 < h < 36 -24 < k < 24 -41 < l < 40
collected reflections		180401	57634
unique reflections		24774	18205
R_{int}		0.1347	0.1217
completeness [%]		99.7	98.9
Max. and min. transmission		0.4749 and 0.3234	0.4573 and 0.3070
refinement method		full-matrix least-squares on F^2	full-matrix least-squares on F^2
data/restraints/parameters		24774/30/818	18205/19/831
GOF on F^2		1.042	1.044
final R indices		R_1 = 0.0486 [$I > 2\sigma(I)$] wR_2 = 0.1343 (all data)	R_1 = 0.0569 [$I > 2\sigma(I)$] wR_2 = 0.1747 (all data)
largest diff peak and hole		2.006 and -2.650 e·A^{-3}	3.284 and -3.839 e·A^{-3}

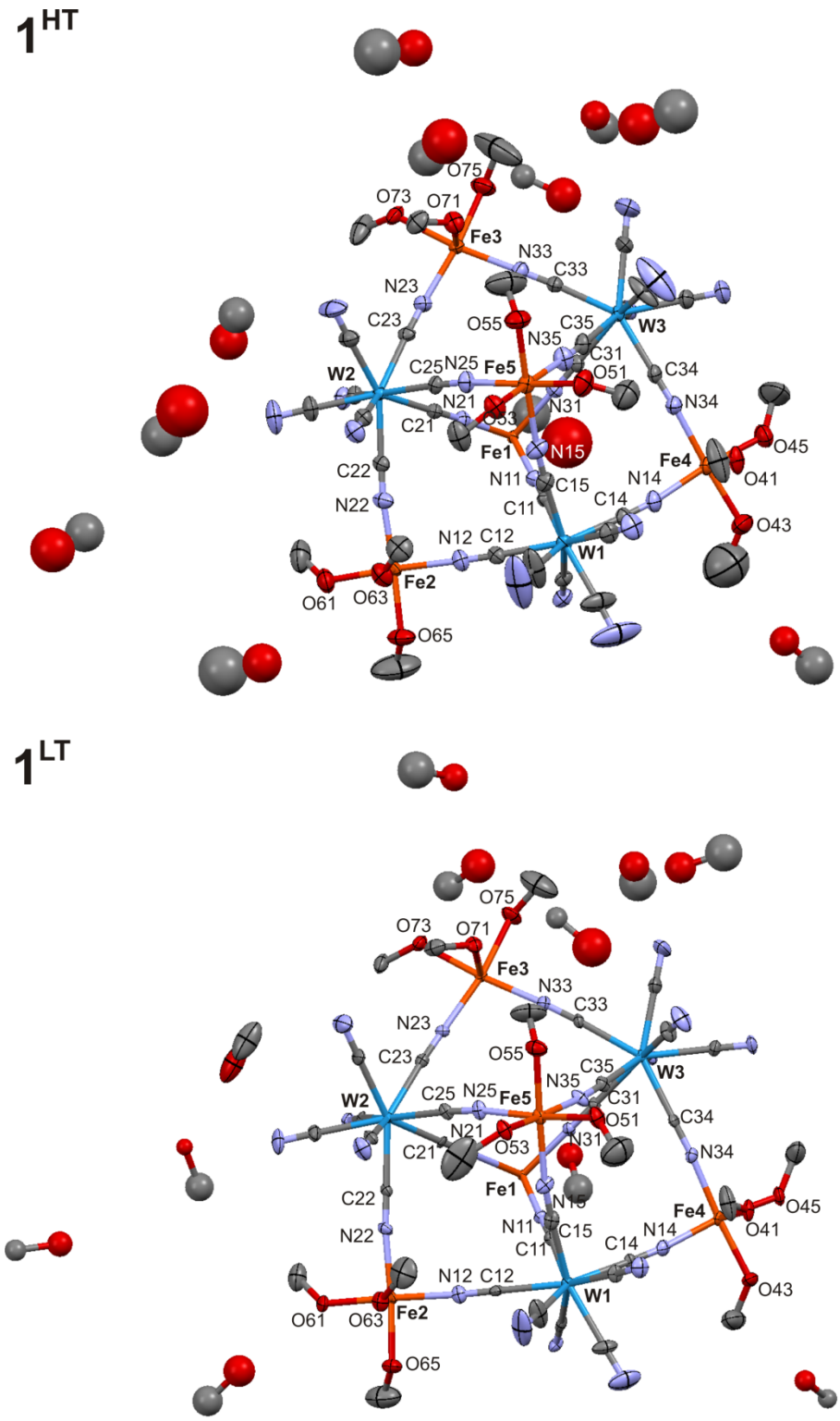

Figure S1. The crystal structure of $\mathbf{1}^{HT}$ and $\mathbf{1}^{LT}$: the asymmetric units with atom labeling scheme. Atom spheres are shown with 40% probability ellipsoids. Labels for atoms are presented only for metal centers, bridging cyanides and oxygen atoms of MeOH ligands. Hydrogen atoms are omitted for clarity.

Table S2 Detailed structure parameters for **1**^{HT} and **1**^{LT}

bond [Å]	**1**^{HT}	**1**^{LT}	angle [deg]	**1**^{HT}	**1**^{LT}
Fe1-N11	2.083(4)	2.042(6)	C11-N11-Fe1	175.6(4)	176.5(7)
Fe1-N21	2.082(4)	2.058(7)	C21-N21-Fe1	176.5(5)	176.8(6)
Fe1-N31	2.071(4)	2.045(6)	C31-N31-Fe1	178.8(5)	179.4(7)
mean Fe1-N	*2.079*	*2.048*	C12-N12-Fe2	178.8(5)	177.2(7)
Fe2-N12	2.121(5)	2.058(7)	C13-N13-Fe2	176.6(5)	173.8(7)
Fe2-N13	2.111(5)	2.057(7)	C22-N22-Fe2	173.9(5)	173.4(7)
Fe2-N22	2.126(5)	2.051(7)	C23-N23-Fe3	175.7(5)	178.3(7)
Fe2-O61	2.148(5)	2.055(6)	C32-N32-Fe3	172.6(5)	170.3(7)
Fe2-O63	2.108(4)	2.020(6)	C33-N33-Fe3	174.6(5)	170.3(7)
Fe2-O65	2.115(5)	2.027(7)	C14-N14-Fe4	173.2(5)	174.5(7)
mean Fe2-N/O	*2.122*	*2.045*	C24-N24-Fe4	173.7(5)	174.5(7)
Fe3-N23	2.135(5)	2.125(7)	C34-N34-Fe4	170.7(5)	173.5(7)
Fe3-N32	2.118(5)	2.091(7)	C15-N15-Fe5	171.2(5)	168.5(7)
Fe3-N33	2.135(5)	2.095(7)	C25-N25-Fe5	172.1(5)	172.1(8)
Fe3-O71	2.117(4)	2.146(6)	C35-N35-Fe5	177.5(6)	174.0(8)
Fe3-O73	2.155(4)	2.133(6)	distance [Å]	**1**^{HT}	**1**^{LT}
Fe3-O75	2.117(5)	2.112(7)	Fe1-W1	5.376	5.345
mean Fe3-N/O	*2.129*	*2.117*	Fe1-W2	5.367	5.333
Fe4-N14	2.128(5)	2.052(8)	Fe1-W3	5.366	5.328
Fe4-N24	2.124(5)	2.050(7)	Fe2-W1	5.404	5.343
Fe4-N34	2.135(5)	2.037(7)	Fe2-W1’	5.414	5.358
Fe4-O41	2.115(4)	2.049(6)	Fe2-W2	5.408	5.325
Fe4-O43	2.109(5)	2.038(6)	Fe3-W2	5.436	5.432
Fe4-O45	2.127(4)	2.042(6)	Fe3-W3	5.407	5.371
mean Fe4-N/O	*2.123*	*2.045*	Fe3-W3’	5.427	5.378
Fe5-N15	2.120(6)	2.094(8)	Fe4-W1	5.401	5.326
Fe5-N25	2.110(5)	2.062(7)	Fe4-W2	5.403	5.317
Fe5-N35	2.125(5)	2.069(8)	Fe4-W3	5.413	5.317
Fe5-O51	2.129(5)	2.092(7)	Fe5-W1	5.413	5.363
Fe5-O53	2.124(4)	2.072(7)	Fe5-W2	5.382	5.330
Fe5-O55	2.117(5)	2.087(7)	Fe5-W3	5.421	5.374
mean Fe5-N/O	*2.121*	*2.079*			

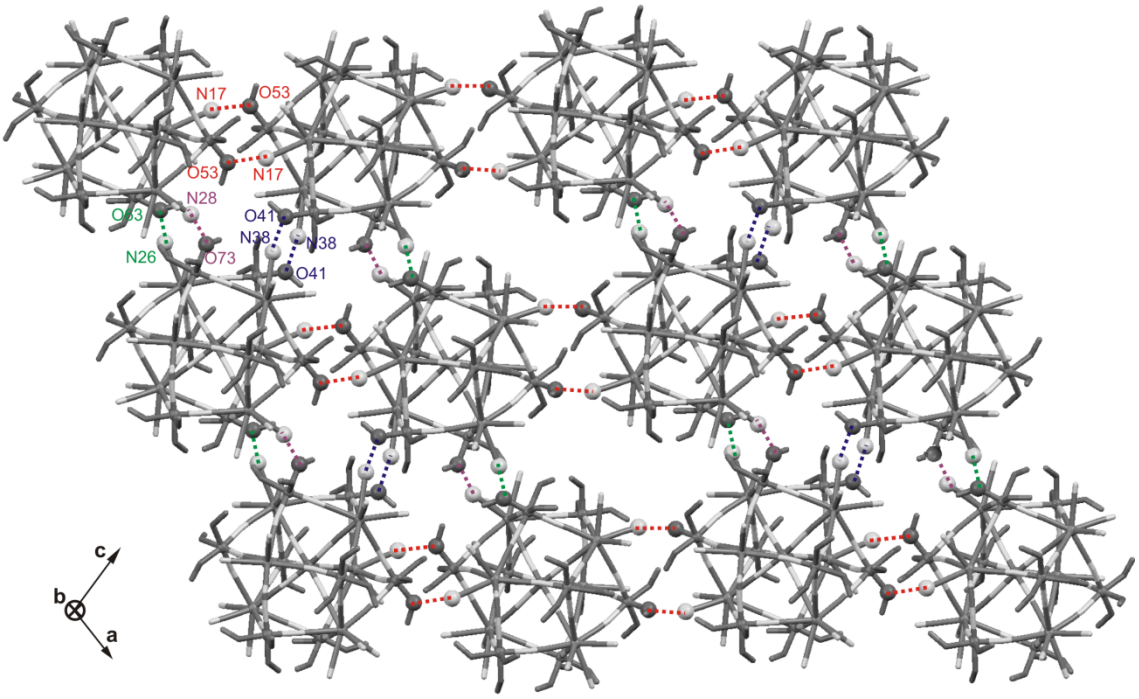

Hydrogen Bonds
Donor-Acceptor distances [Å]

Atom labels	$\mathbf{1}^{HT}$	$\mathbf{1}^{LT}$
O53 – N17	2.76	2.70
O63 – N26	2.74	2.59
O73 – N28	2.79	2.70
O41 – N38	2.75	2.67

Figure S2. The crystal structure of $\mathbf{1}^{HT}$ and $\mathbf{1}^{LT}$: the hydrogen bonding network together with donor-acceptor distances. The strongest direct intercluster hydrogen bonds are realized through interactions between coordinated methanol molecules and terminal cyanides. The closest contacts are observed within *ac* plane, whereas the distances between clusters along *b* axis are definitely longer. The general two-dimensional character of hydrogen bonding network is preserved during the transition, only the corresponding intercluster distances become much smaller in $\mathbf{1}^{LT}$.

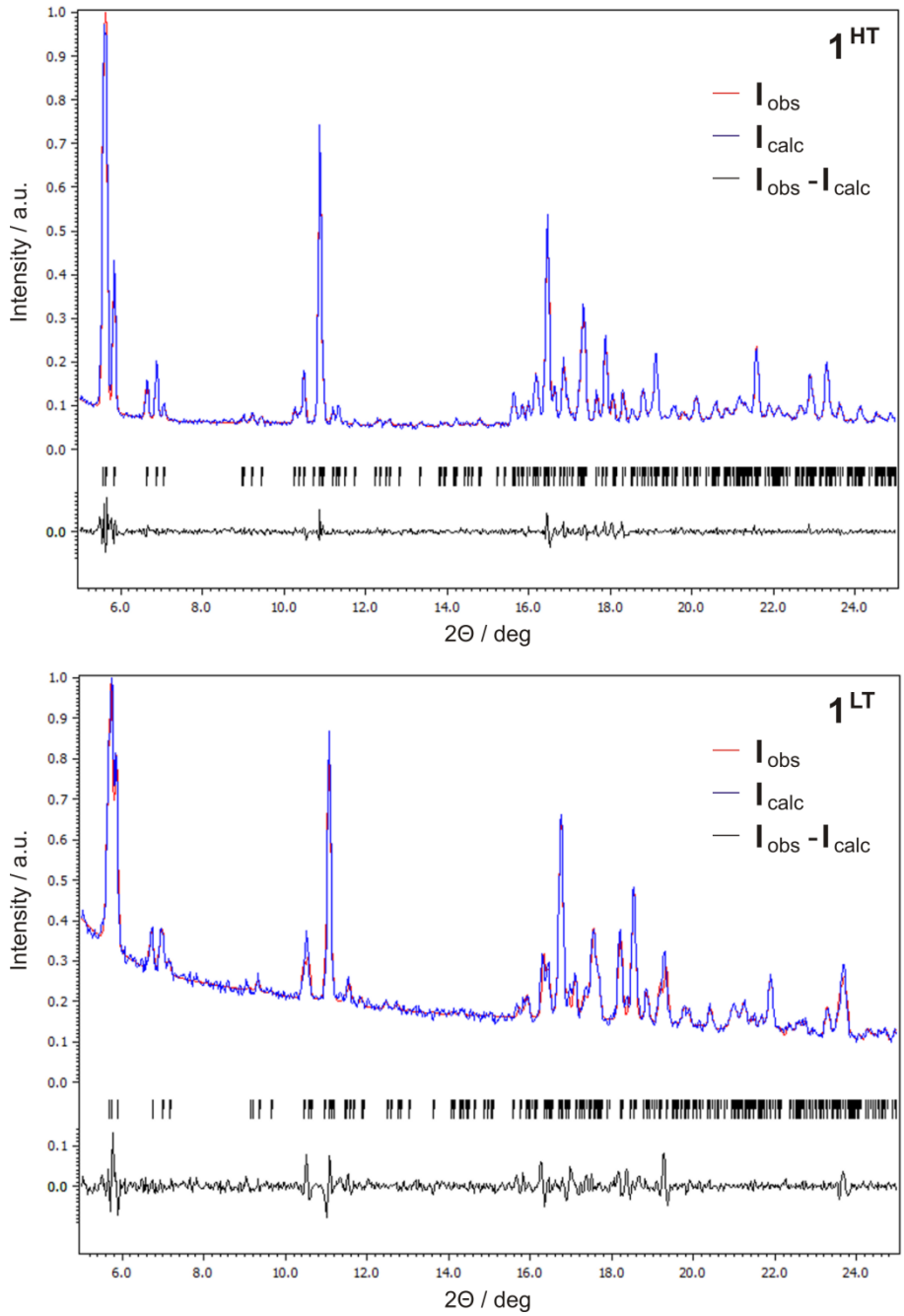

phase	space group	***a*** [Å]	***b*** [Å]	***c*** [Å]	***β*** [deg]	V [Å^3]	GOF	R_p	wR_p
1^{HT}	C 2/c	28.8431(11)	19.5693(5)	32.7628(10)	113.588(3)	16947.5(9)	0.83	3.73	5.33
1^{LT}	C 2/c	28.1046(3)	19.0224(3)	32.2271(4)	113.4661(8)	15804.2(6)	1.14	3.85	5.42

Figure S3. The PXRD analysis for phase transition in **1@MeOH**: the Rietveld plots for indexing of diffractograms of **1^{HT}** and **1^{LT}** together with the unit cell parameters for both phases.

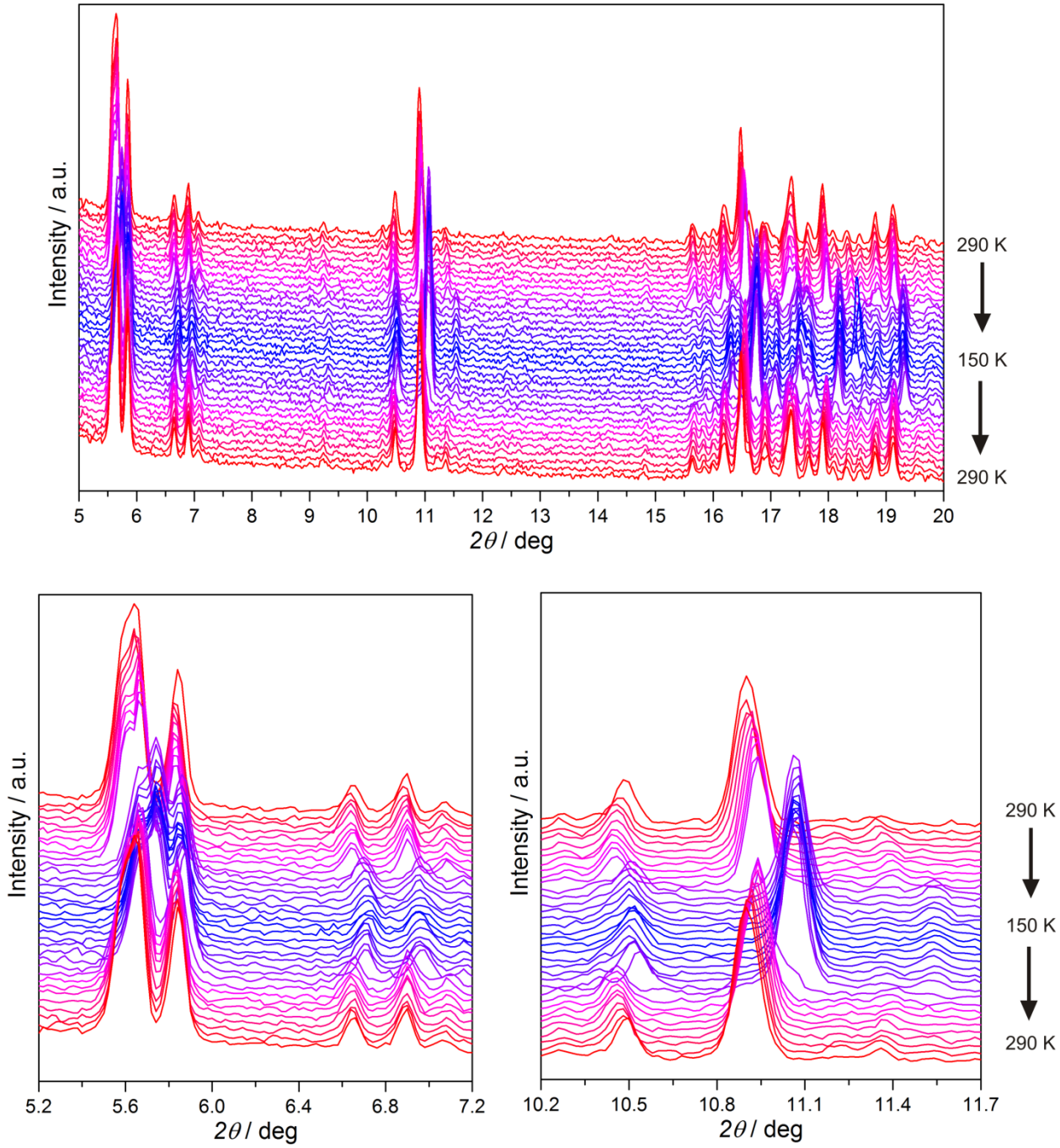

Figure S4. The PXRD analysis for phase transition in **1@MeOH**: the thermal evolution of powder diffractogramms (5 – 20° range) for the 290 K → 150 K → 290 K sequence (top) with the insight into temperature dependence of the selected PXRD peaks (bottom). Peak for $2\Theta \sim 11°$ corresponds to the distance between $(22\bar{1})$ layers, and was used in the analysis of phase transition occurring in **1** (*see* Figure 2).

Table S3. The spectroscopic characterization of phase transition in **1@ap**: the isomeric shift IS and quadrupole QS parameters for Mössbauer spectra of $\mathbf{1}^{\mathbf{HT}}$ and $\mathbf{1}^{\mathbf{LT}}$

phase	doublet	relative intensity [%]	IS [mm·s^{-1}]	QS [mm·s^{-1}]	assignment
$\mathbf{1}^{\mathbf{HT}}$	1	19.44	1.394(3)	0.876(2)	$^{HS}Fe^{II}$
	2	55.92	1.002(4)	0.775(3)	$^{HS}Fe^{II}$
	3	24.64	0.284(2)	0.482(2)	$^{HS}Fe^{III}$
$\mathbf{1}^{\mathbf{LT}}$	1	31.84	1.162(4)	1.539(3)	$^{HS}Fe^{II}$
	2	68.16	0.412(3)	0.173(2)	$^{HS}Fe^{III}$

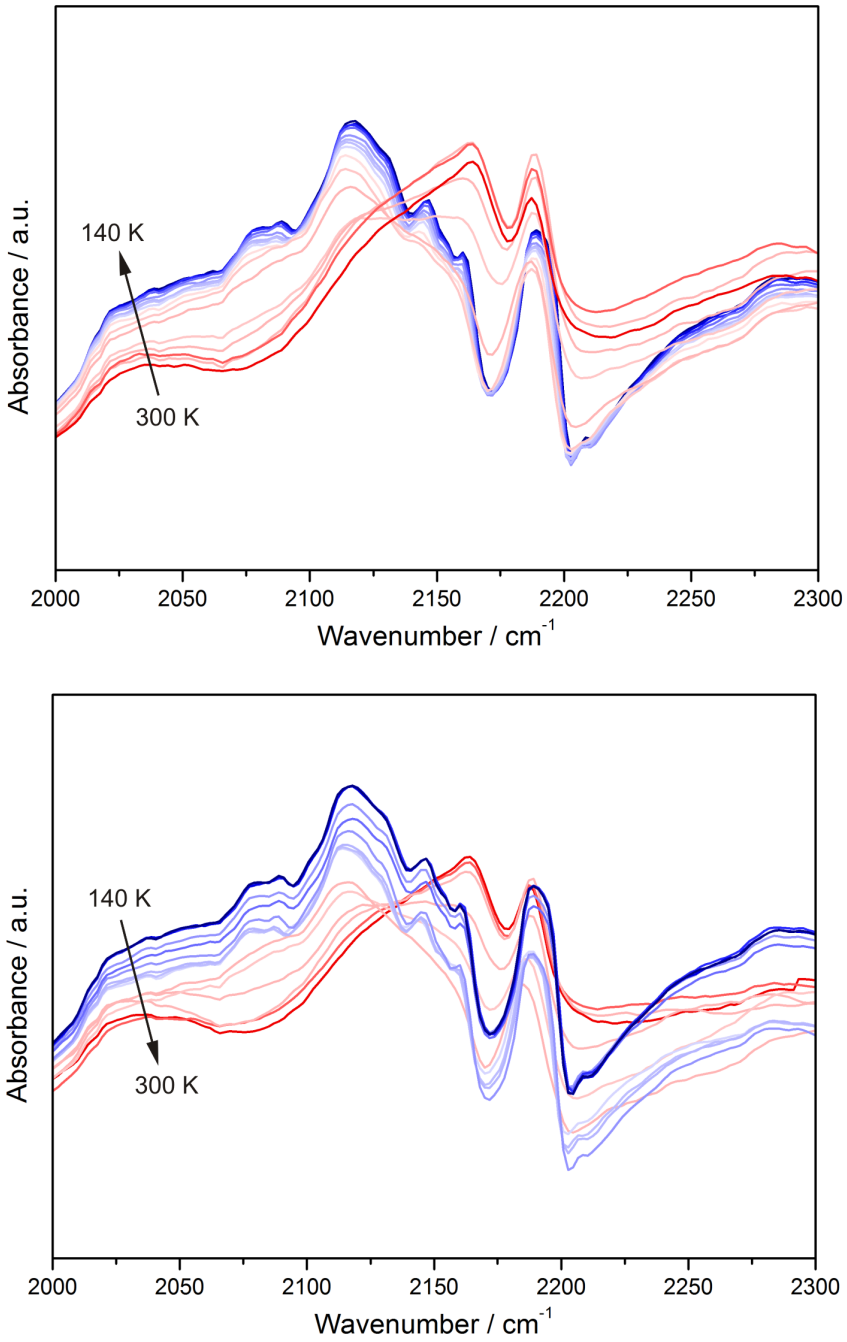

Figure S5. The overview of temperature dependence of IR spectra of **1@ap** in ν(CN) region in 140 - 300 K range on cooling (top) and heating (bottom).

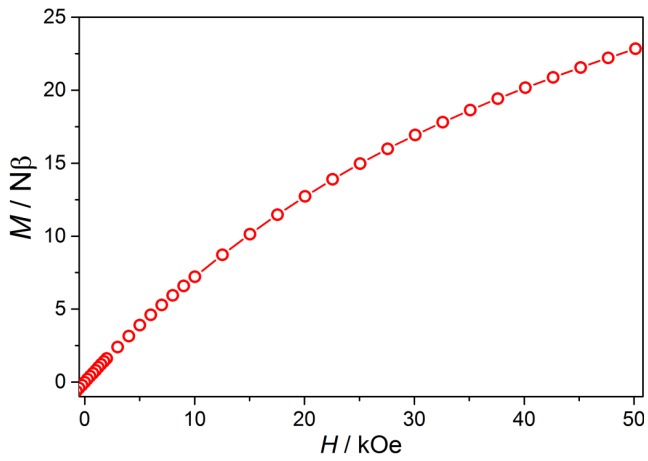

Figure S6. Additional magnetic characteristic for **1@MeOH**: magnetization versus applied magnetic field curve in the 0 – 50 kOe range at T = 2 K

Comment to magnetic properties of **1**:

The $\chi_M T(T)$ signal for **1@MeOH** at 298 K is equal to 37.3 $cm^3 \cdot K \cdot mol^{-1}$ which is within the range of 35.6 – 38.0 $cm^3 \cdot K \cdot mol^{-1}$ calculated for uncoupled $(^{HS}Fe^{II})_7(^{HS}Fe^{III})_2(W^{IV})_2(W^{V})_4$ unit of $\mathbf{1}^{HT}$ suggested by ^{57}Fe Mössbauer spectra. In this calculation, we assume the spins of $S(Fe^{II\text{-}HS}) = 2$, $S(Fe^{III\text{-}HS}) = 5/2$, $S(W^{V}) = 1/2$, and the Fe^{III}-HS *g*-factor of 2.0. For $[W^{V}(CN)_8]^{3-}$ ions, we assume the average *g*-factor of 1.97 as was found in ESR spectra in its inorganic salts and some coordination systems.[S7-S9] The *g*-factor of high-spin Fe^{II} complexes was assumed to be in the range of 2.2 – 2.3 as observed in other cyanido-bridged systems containing these centers.[S10-S12]

On cooling, the signal decrease very slowly to 35.9 $cm^3 \cdot K \cdot mol^{-1}$ at 230 K, then increase rapidly to 36.6 $cm^3 \cdot K \cdot mol^{-1}$ at 205 K (Fig. 5). On further cooling, it starts to decrease slowly down to 50 K, and faster below this point. During the heating, the signal follows the cooling line, however the hysteresis appears with $T_{c\downarrow} = 208$ K and $T_{c\uparrow} = 215$ K. It has very small amplitude and specific reversed character with $\chi_M T(T)$ signal higher for $\mathbf{1}^{LT}$ than for $\mathbf{1}^{HT}$. This definitely suggests the $^{HS}Fe^{II}W^{V} \rightarrow {}^{HS}Fe^{III}W^{IV}$ electron transfer. For such process, the $\chi_M T(T)$ signal is expected to change very slightly from ca. 4.00 $cm^3 \cdot K \cdot mol^{-1}$ calculated for one pair of $^{HS}Fe^{II}$-W^{V} centers to 4.375 $cm^3 \cdot K \cdot mol^{-1}$ calculated for a pair of $^{HS}Fe^{III}$-W^{IV} centers. The change of $\chi_M T$ connected with the transition is ca. 1.2 $cm^3 \cdot K \cdot mol^{-1}$ which is only slightly smaller than expected 1.5 $cm^3 \cdot K \cdot mol^{-1}$ for the transition producing four new $^{HS}Fe^{III}W^{IV}$ pairs as suggested by ^{57}Fe Mössbauer spectra. However, the general increase of $\chi_M T$ on cooling excludes the possibility of spin transition as the appearance of low-spin states of Fe^{II} (S = 0) or Fe^{III} (S = 1/2) should obviously lead to the dramatic decrease of $\chi_M T$. The $M(H)$ signal at $T = 2$ K does not saturate up to 50 kOe, reaching the value of 22.1 Nβ, which is significantly lower than 37.1 Nβ expected for the tentative $(^{HS}Fe^{III})_6(^{HS}Fe^{II})_3(W^{IV})_6$ composition of $\mathbf{1}^{LT}$ (Fig. S6). This together with the shape of $\chi_M T(T)$ curve suggests that the antiferromagnetic interactions operate, however the single-ion features and weak intermolecular interactions should also be taken into account. No long-range magnetic ordering was observed down to 1.8 K.

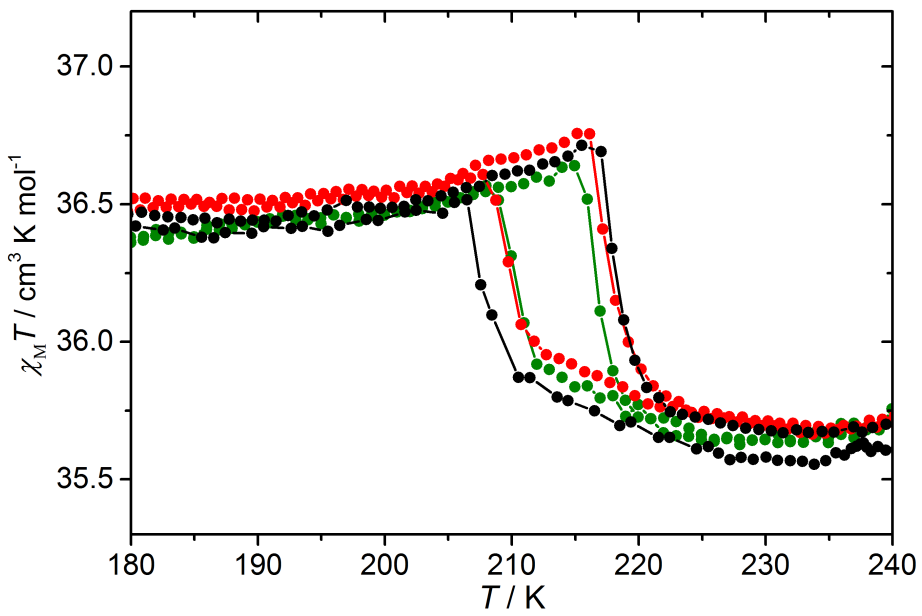

Figure S7. Magnetic susceptibility (shown as $\chi_M T$ product) of **1@MeOH** measured at 1 kOe using different temperature sweep rates: 2 K·min^{-1} (black), 1 K·min^{-1} (red), and for stabilized temperature at each point – rate about 0.1 K·min^{-1} (green). The sample was cycled three times between 170 and 260 K during this measurement, and this does not change significantly the transition temperatures, nor the shape of the hysteresis.

References to Supporting Information

(S1) A. Samotus, *Pol. J. Chem*., 1973, **47**, 653.

(S2) A. Altomare, M. C. Burla, M. Camalli, G. L. Cascarano, C. Giacovazzo, A. Guagliardi, A. G. G. Moliterni, G. Polidori and R. Spagna, *J. Appl. Cryst*. 1999, **32**, 115.

(S3) G. M. Sheldrick, *Acta Cryst*. 2008, **A64**, 112.

(S4) C. F. Macrae, P. R. Edgington, P. McCabe, E. Pidcock, G. P. Shields, R. Taylor, M. Towler, and J. van de Streek, *J. Appl. Cryst*. 2006, **39**, 453.

(S5) V. Petricek, M. Dusek and L. Palatinus, Jana2006, 2006. The crystallographic computing system. Institute of Physics, Praha, Czech Republic.

(S6) G. A. Bain and J. F. Berry, *J. Chem. Edu*., 2008, **85**, 532.

(S7) R. A. Pribush and R. D. Archer, *Inorg. Chem*., 1974, **13**, 2556.

(S8) E. Chelebaeva, J. Long, J. Larionova, R. A. S. Ferreira, L. D. Carlos, F. A. Almeida Paz, J. B. R. Gomes, A. Trifonov, C. Guerin and Y. Guari, *Inorg. Chem*., 2012, **51**, 9005.

(S9) N. Ozaki, H. Tokoro, Y. Hamada, A. Namai, T. Matsuda, S. Kaneko and S. Ohkoshi, *Adv. Funct. Mater*., 2012, **22**, 2089.

(S10) M. Arai, W. Kosaka, T. Matsuda and S. Ohkoshi, *Angew. Chem. Int. Ed*., 2008, **47**, 6885.

(S11) W. Kosaka, H. Tokoro, T. Matsuda, K. Hashimoto and S. Ohkoshi, *J. Phys. Chem. C*, 2009, **113**, 15751.

(S12) D. Pinkowicz, R. Podgajny, R. Pełka, W. Nitek, M. Bałanda, M. Makarewicz, M. Czapla, J. Żukrowski, C. Kapusta, D. Zając and B. Sieklucka, *Dalton Trans*., 2009, 7771.